

Quantization of the band at the surface of charge density wave material 2H-$TaSe_2$

Man Li(李满)†, Nan Xu(徐楠)†, Jianfeng Zhang(张建丰)†, Rui Lou(娄睿), Ming Shi(史明), Lijun Li(黎丽君), Hechang Lei(雷和畅), Cedomir Petrovic, Zhonghao Liu(刘中灏), Kai Liu(刘凯), Yaobo Huang(黄耀波)‡, and Shancai Wang(王善才)§

Citation: Chin. Phys. B, 2021, 30 (**4**): 047305. DOI: 10.1088/1674-1056/abe9a8
Journal homepage: http://cpb.iphy.ac.cn; http://iopscience.iop.org/cpb

What follows is a list of articles you may be interested in

Epitaxial fabrication of monolayer copper arsenide on Cu(111)

Shuai Zhang(张帅), Yang Song(宋洋), Jin Mei Li(李金梅), Zhenyu Wang(王振宇), Chen Liu(刘晨), Jia-Ou Wang(王嘉鸥), Lei Gao(高蕾), Jian-Chen Lu(卢建臣), Yu Yang Zhang(张余洋), Xiao Lin(林晓), Jinbo Pan(潘金波), Shi Xuan Du(杜世萱), Hong-Jun Gao(高鸿钧)

Chin. Phys. B, 2020, 29 (**7**): 077301. DOI: 10.1088/1674-1056/ab8db3

Electronic structure of correlated topological insulator candidate YbB_6 studied by photoemission and quantum oscillation

T Zhang(张腾), G Li(李岗), S C Sun(孙淑翠), N Qin(秦娜), L Kang(康璐), S H Yao(姚淑华), H M Weng(翁红明), S K Mo, L Li(李璐), Z K Liu(柳仲楷), L X Yang(杨乐仙), Y L Chen(陈宇林)

Chin. Phys. B, 2020, 29 (**1**): 017304. DOI: 10.1088/1674-1056/ab6206

Electronic structure of molecular beam epitaxy grown 1T'-$MoTe_2$ film and strain effect

Xue Zhou(周雪), Zeyu Jiang(姜泽禹), Kenan Zhang(张柯楠), Wei Yao(姚维), Mingzhe Yan(颜明哲), Hongyun Zhang(张红云), Wenhui Duan(段文晖), Shuyun Zhou(周树云)

Chin. Phys. B, 2019, 28 (**10**): 107307. DOI: 10.1088/1674-1056/ab43ba

Tight-binding electron-phonon coupling and band renormalization in graphene

Zhang De-Sheng, Kang Guang-Zhen, Li Jun

Chin. Phys. B, 2015, 24 (**1**): 017301. DOI: 10.1088/1674-1056/24/1/017301

Topological edge states and electronic structures of a 2D topological insulator: Single-bilayer Bi (111)

Gao Chun-Lei, Qian Dong, Liu Can-Hua, Jia Jin-Feng, Liu Feng

Chin. Phys. B, 2013, 22 (**6**): 067304. DOI: 10.1088/1674-1056/22/6/067304

RAPID COMMUNICATION

Quantization of the band at the surface of charge density wave material 2H-$TaSe_2$*

Man Li(李满)[1,2,†], Nan Xu(徐楠)[3,†], Jianfeng Zhang(张建丰)[1,†], Rui Lou(娄睿)[1], Ming Shi(史明)[4], Lijun Li(黎丽君)[5], Hechang Lei(雷和畅)[1], Cedomir Petrovic[6], Zhonghao Liu(刘中灏)[7], Kai Liu(刘凯)[1], Yaobo Huang(黄耀波)[2,‡], and Shancai Wang(王善才)[1,§]

[1] *Department of Physics and Beijing Key Laboratory of Opto-electronic Functional Materials & Micro-nano Devices, Renmin University of China, Beijing* 100872, *China*

[2] *Shanghai Synchrotron Radiation Facility, Shanghai Institute of Applied Physics, Chinese Academy of Sciences, Shanghai* 201204, *China*

[3] *Institute of Advanced Studies, Wuhan University, Wuhan* 430072, *China*

[4] *Swiss Light Source, Paul Scherrer Institute, CH-*5232 *Villigen, Switzerland*

[5] *Chongqing Technology and Busineee University, Chongqing* 400067, *China*

[6] *Condensed Matter Physics and Materials Science Department, Brookhaven National Laboratory, Upton, NY* 11973, *USA*

[7] *State Key Laboratory of Functional Materials for Informatics and Center for Excellence in Superconducting Electronics, SIMIT, Chinese Academy of Sciences, Shanghai* 200050, *China*

(Received 13 January 2021; revised manuscript received 8 February 2021; accepted manuscript online 25 February 2021)

By using angle-resolved photoemission spectroscopy (ARPES) combined with the first-principles electronic structure calculations, we report the quantized states at the surface of a single crystal 2H-$TaSe_2$. We have observed sub-bands of quantized states at the three-dimensional Brillouin zone center due to a highly dispersive band with light effective mass along k_z direction. The quantized sub-bands shift upward towards E_F while the bulk band at Γ shifts downward with the decrease of temperature across charge density wave (CDW) formation. The band shifts could be intimately related to the CDW. While neither the two-dimensional Fermi-surface nesting nor purely strong electron–phonon coupling can explain the mechanism of CDW in 2H-$TaSe_2$, our experiment may ignite the interest in understanding the CDW mechanism in this family.

Keywords: angle-resolved photoemission spectroscopy, transition metal dichalcogenide, $TaSe_2$

PACS: 73.20.–r, 79.60.–i, 73.20.Mf **DOI:** 10.1088/1674-1056/abe9a8

1. Introduction

Manipulation of two-dimensional electron gas (2DEGS) has recently drawn considerable interest.[1–4] As a mechanism for tailoring the many-body interactions, 2DEGS is embodied in the interface of semiconductors[5–7] and metal-films.[8–10] This has attracted a lot of interests due to observation of high electron mobility,[11,12] quantum Hall effect,[13,14] superconductivity,[15] large magnetoresistance,[16] etc. The 2DEGS is generally caused by the confinement of electrons along one dimension, for example, by the depletion of charge carriers close to the surface and then inducing a band-bending to confine the electrons into 2DEGS.[17] Due to the shielding effect of good conductors, it is difficult to achieve 2DEG in metals. Monolayer transition metal dichalcogenides (TMDs) MX_2 (M = Mo, W; X = S, Se) represent a natural host for 2DEGS.[18]

The mechanism of CDW in quasi-two-dimensional TMDs is a controversial topic for a few decades. Both weak-coupling approaches and strong coupling mean-field models have been proposed, e.g., the Fermi surface (FS) nesting,[19–21] saddle point,[22–24] local chemical bonds,[25,26] excitonic insulator,[27–29] and lattice-driven models,[30–32] however, no consensus has been reached in the driving mechanism of the CDW in TMDs. On the other hand, there is coexistence/competition between the CDW and superconductivity[33,34] in many TMDs. Thus the understanding of the CDW mechanism remains a challenge.

The 2H-$TaSe_2$ consists of three-atom-thick chalcogen-transition metal-chalcogen sandwiches and its unit cell can be considered as two layers of Ta-Se with a 60° rotation with van der Waals' force in adjoining layers.[33] 2H-$TaSe_2$ undergoes a second-order transition from normal phase to an incommensurate ordered phase at T = 122 K, followed by a first-order lock-in transition to a 3×3 commensurate CDW (CCDW) phase at T_{CDW} = 90 K.[33,35] The CDW mechanism in 2H-$TaSe_2$

*Project supported by the National Natural Science Foundation of China (Grant Nos. 11774421, 11774424, 11574394, 11774423, 11822412, and 11874047), the National Key R&D Program of China (Grant Nos. 2016YFA0401002, 2018YFA0307000, 2016YFA0300504, and 2018FYA0305800), and the Fundamental Research Funds for the Central Universities, China (Grant No. 2042018kf-0030).

†These authors contributed equally.

‡Corresponding author. E-mail: huangyaobo@zjlab.org.cn

§Corresponding author. E-mail: scw@ruc.edu.cn

© 2021 Chinese Physical Society and IOP Publishing Ltd

has been investigated experimentally by ARPES, STM, transport measurement, neutron scattering,[20,21,35–44] and band structure calculations.[45–47] Recently, the k-dependence of susceptibility and k-integrated function calculations disagree with the CDW wave vectors in 2H-$TaSe_2$ and the FS nesting scenario is excluded as a driven force.[32,45,48] The strong electron–phonon coupling with wave-vector-dependent electron–phonon matrix elements[30,32] and a new type of collective excitation[37] as the condensation of preformed excitons[49] are proposed, but further evidence is needed.

In this paper, we report an ARPES study of the electronic structure of 2H-$TaSe_2$ with various photon energies in the compensate CDW state and normal state. In addition to the 2D-like band structure reported before, we report a quantized state induced by the intrinsic band structure at Brillouin zone center (Γ) below E_F in 2H-$TaSe_2$ single crystal for the first time. It is formed by a band with strong k_z dispersion and approaches E_F near 3D BZ center predicted in the bulk band calculation, but not reported in the ARPES measurement before. The combination of near-surface band-bending potential created by the rearrangement of surface electrons and the light effective mass along k_z direction causes the quantization along c-axis and the formation of the manifold sub-bands at the surface, similar to that in semiconductors.[17] With the decrease of temperature below T_{CDW}, the sub-bands shift upward while most of the bulk bands show no noticeable change. This abnormal band shift may be related to the CDW but could not be explained yet. When neither the model of Fermi surface nesting nor the electron–phonon coupling could successfully explain the origin of CDW in 2H-$TaSe_2$, our discovery and extensive analysis of those results may unlock new perspectives and avenues for understanding the CDW mechanism.

2. Materials and methods

Single crystals of 2H-$TaSe_2$ were grown by the iodine vapor transport method. The element analysis and transport measurement of the samples indicate the high quality of crystals in this paper.[33] ARPES measurement was performed at the Dreamline beamline of the Shanghai Synchrotron Radiation Facility with a Scienta D80 analyzer and at the SIS-HRPES beamline of the Swiss Light Source with a Scienta R4000 analyzer. The energy and angular resolutions were better than 15 meV and 0.2°, respectively. The sample for the ARPES measurements was cleaved *in situ* along (001) direction in a vacuum better than 5×10^{-11} Torr. Normal and CDW phases measurements were taken at $T = 150$ K and $T = 20$ K, respectively. The electronic structure of 2H-$TaSe_2$ was studied by using first-principles calculations with the projector augmented wave (PAW) method[50,51] as implemented in the VASP package.[52–54] For the exchange–correlation functional, the generalized gradient approximation (GGA) of the Perdew–Burke–Ernzerhof (PBE) formula[55] was adopted. The kinetic energy cutoff of the plane-wave basis was set to be 300 eV. A $16 \times 16 \times 4$ k-point mesh was utilized for the Brillouin zone (BZ) sampling and the Fermi surface was broadened by the Gaussian smearing method with a width of 0.05 eV. The vdW interactions between the $TaSe_2$ layers were considered by adopting the optB86b-vdW functional.[56] The lattice parameters and internal atomic positions were fully relaxed until the forces on all atoms were smaller than 0.01 V/Å. After the equilibrium structures were obtained, the electronic structures were calculated by including the spin–orbit-coupling (SOC) effect. In the slab calculation, a two-dimensional supercell with a 21-layer $TaSe_2$ slab and a 20-Å vacuum was employed.

3. Results and discussion

The schematic bulk BZ is presented in Fig. 1(a). We performed the band calculation along high symmetry lines of 3D BZ, as shown in Fig. 1(b). Two Ta-d bands, split by the bi-(Ta-Se) layers, labeled as α and β, crossing E_F along high symmetry lines are shown in Fig. 1(b).[45,47] Figures 1(c) and 1(d) demonstrate the FS topologies of 2H-$TaSe_2$ at temperatures below ($T = 20$ K) and above ($T = 150$ K) commensurate CDW transition temperature, respectively, with photon energy $h\nu = 50$ eV, which corresponds to the Γ–M–K plane and is indicated as the color plane in Fig. 1(a). We observe two hole-pockets centered at $\bar{\Gamma}$ and $\bar{K}$, respectively, and a "dog-bone" shaped electron-pocket centered at $\bar{M}$ in the normal state (Fig. 1(d)). A "pseudogap" of unclear origin has been reported at $\bar{K}$-centered FS by the suppression of the spectral weight at $T \gg T_{CDW}$.[20,21] At the low temperature in the CCDW state, as illustrated in Figs. 1(c), the $\bar{K}$-centered pocket completely loses its weight at E_F, whereas the $\bar{M}$-centered pocket is only partially gaped, forming triangular FS pockets.[21] We extract the Fermi wave vectors from the ARPES experimental data above T_{CDW} and plot them in Fig. 1(e). The extracted FS data are in agreement with early studies.[20,21,36,37]

The temperature dependence of the gap is shown in Fig. 2. Figures 2(a) and 2(b) show the intensity plots along $\bar{K}$–$\bar{M}$–$\bar{K}$ at the CCDW state ($T = 10$ K) and normal state ($T = 160$ K), respectively. From the plots, we can see a band across E_F at #a, which forms the dog-bone shaped FS around $\bar{M}$ point both at the CDW and normal states, with no gap opening observed. For the band close to #b, which forms the circular FS around $\bar{K}$ point in Fig. 1, it shows a clear bending back and a gap feature at low temperature, as shown in Fig. 2(a). At the normal state, the intensity becomes faint but the back bending and the gap feature remain. To illustrate the gap evolution, the symmetrized energy distribution curves (EDCs) at the crossing points are shown in Figs. 2(c) and 2(d) for crossing points #a and #b, respectively. For #a, the symmetrized EDCs

show a small peak centered at E_F, suggesting a well-defined quasiparticle peak at low temperature. The intensity decreases with the increase of temperature and diminishes at around 90 K. For #b, the symmetrized EDCs show a clear double-peak feature at low temperature, showing a CDW gap of about $\sim 90 \pm 10$ meV. With the increase in temperature, the peak intensity decreases but the gap remains across the T_{CDW}, forming a "pseudogap" up to room temperature. We extract the full gap (2Δ) from the separation of two symmetrical quasiparticle peaks, and plot the gap values at different temperatures in Fig 2(e). The maximum CDW gap 90±10 meV fits well with the previous STM measurements.[40] Having fully characterized the gap variation with the temperature around $\bar{K}$, we also study the gap variation with momentum position around $\bar{M}$ at $T = 20$ K, as shown in Fig. 2(f). At $\bar{M}$ pocket, four energy-gap nodes can be found at loin and apex of the "dog-bone shaped" FS corresponding to $\theta \sim 0$, $\pi/2$, $3\pi/2$, and 2π, respectively. The maximum energy gap locates at about $\pm\pi/4$ and $\pm 3\pi/4$.

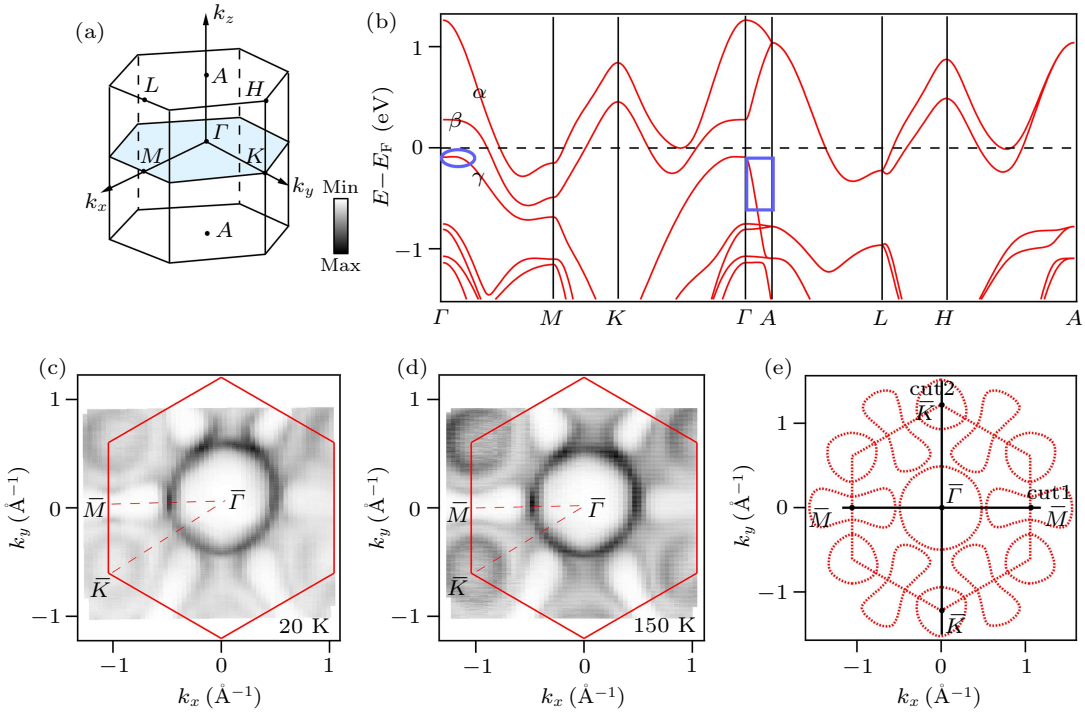


Fig. 1. Brillouin zone and Fermi surface of 2H-$TaSe_2$. (a) 3D bulk BZ with marked high-symmetry points and a colored high symmetry plane. (b) Calculated bulk band structure along high-symmetry lines including SOC. Three near-E_F bands are denoted as α, β, and γ, respectively. (c), (d) Integrated intensity plots within $E_F \pm 10$ meV at $T = 20$ K and 150 K to show the FS topology, obtained with $h\nu = 50$ eV showing the colored plane indicated in (a), corresponding to CDW and normal phase, respectively. (e) The extracted ARPES mapping in the normal state. Marked cuts #1 and #2 indicate the momentum locations of the measured bands in Fig. 3.

The in-plane band dispersion along high symmetry directions is shown in Fig. 3. Two major momentum cuts ($\bar{\Gamma}$–$\bar{M}$ and $\bar{\Gamma}$–$\bar{K}$) with photon energies $h\nu = 50$ eV ($k_z \sim 0$), indicated as cuts #1 and #2 in Fig. 1(e), are shown respectively. Along the $\bar{\Gamma}$–$\bar{M}$ direction, we can observe a hole-like band across E_F at both below and above the T_{CDW}. According to the bulk band calculation, two bands (α, β) across E_F along Γ–M, and are nearly degenerate along A–L. From Figs. 3(a) and 3(b), the two bands are nearly degenerate and only become separable near M point at about $E_B \sim 300$–400 meV. No observable change near E_F (band shifts or gap opening) is identified through the CDW transition along this direction. A 3×3 reconstruction below T_{CDW} has been reported[21] in 2H-$TaSe_2$ and some faint shadow bands could be barely seen in the second derivative plots. The agreement between the ARPES results along $\bar{\Gamma}$–$\bar{K}$ (Figs. 3(f)–3(j)) and the bulk band calculation is similar as those along $\bar{\Gamma}$–$\bar{M}$, except the opening gap of CDW close to $\bar{K}$ point.

A major difference between the observation and the bulk band calculation is the existence of quantized states from the "missing" γ band which was not experimentally reported before. In the bulk band structure calculation [blue ellipse in Fig. 1(b)], there is a hole-like band near the Brillouin zone center close to E_F. Instead, we observe several replica bands with the band top at about $E_B \approx 460$ meV below E_F, which can be visualized from the intensity plot (Figs. 3(a), 3(d), 3(f), and 3(i)) and the corresponding second derivative plot (Figs. 3(b), 3(e), 3(g), and 3(j)). We attribute the quantized states to the surface bands caused by the breaking of translation symmetry along the c-axis, and the light effective mass of the band along this direction (Γ–A). The topmost few layers/vacuum interfaces could induce a spatial redistribution of carriers, leading to the bending of the electronic bands relative to the Fermi level,[17] and forming a quantized state near the sample surface. To estimate the γ band dispersion along k_z, we plot the

ARPES intensity data in Fig. 4(c), and estimate the band dispersion with the influence of quantization. The effective mass $m_z^* \approx 0.06m_e$ is extracted from a parabolic fit to the dispersion. We also note that the in-plane band masses estimated from the band dispersion along k_x and k_y are approximately $0.23m_e$ and $0.31m_e$, respectively, much higher than that along k_z. The surface quantizations are caused by downward shift of the near-surface band potential, which thus confines the electronic-state-wavefunction along k_z-direction, forming the quantized in-plane bands, similar to $SrTiO_3$, InN, and $PtSe_2$.[2,6,58]

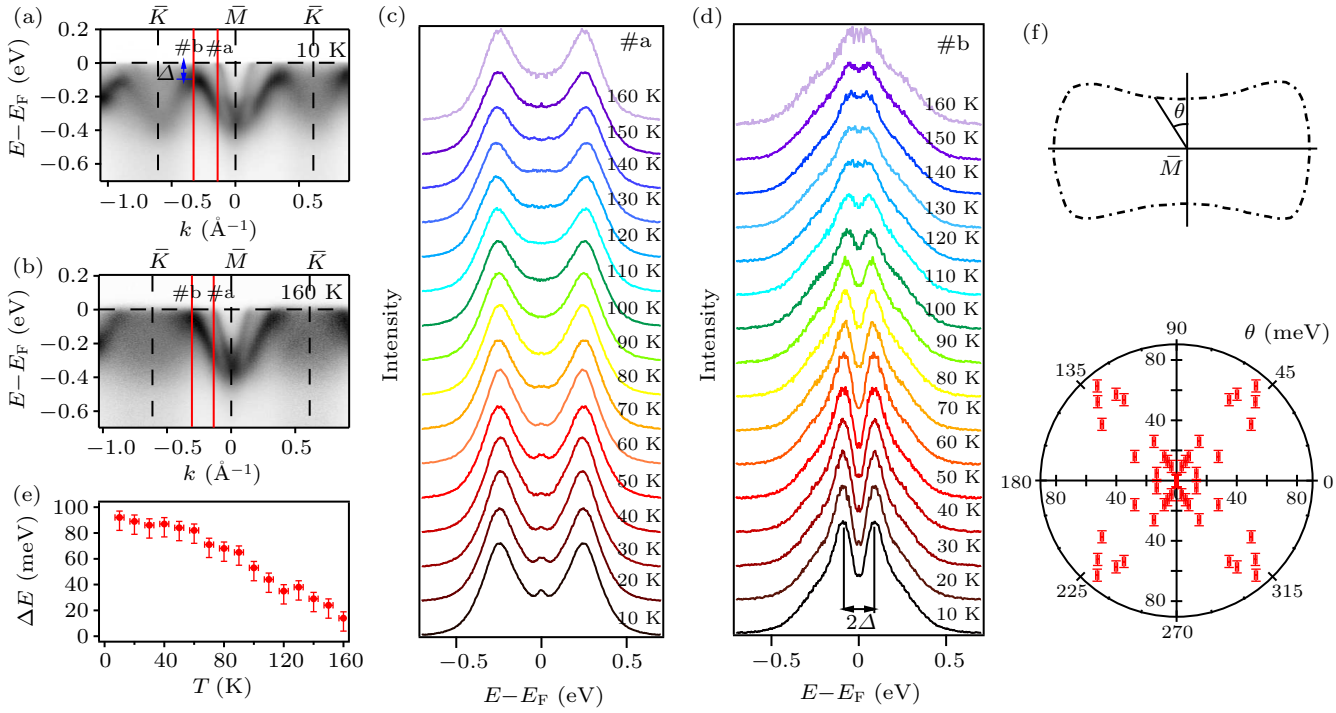


Fig. 2. Temperature dependence of band gap. (a) The band dispersion along the direction of $\bar{K}$–$\bar{M}$–$\bar{K}$ at $T = 10$ K, Δ is the CDW gap. (b) Same as (a), but displayed at $T = 160$ K. (c), (d) The temperature dependence of symmetrized EDCs along the momentum marked by #a and #b, respectively. (e) The extracted band gap (Δ) as a function of temperature. (f) The gap varies with momentum position (θ) at $\bar{M}$ pocket.

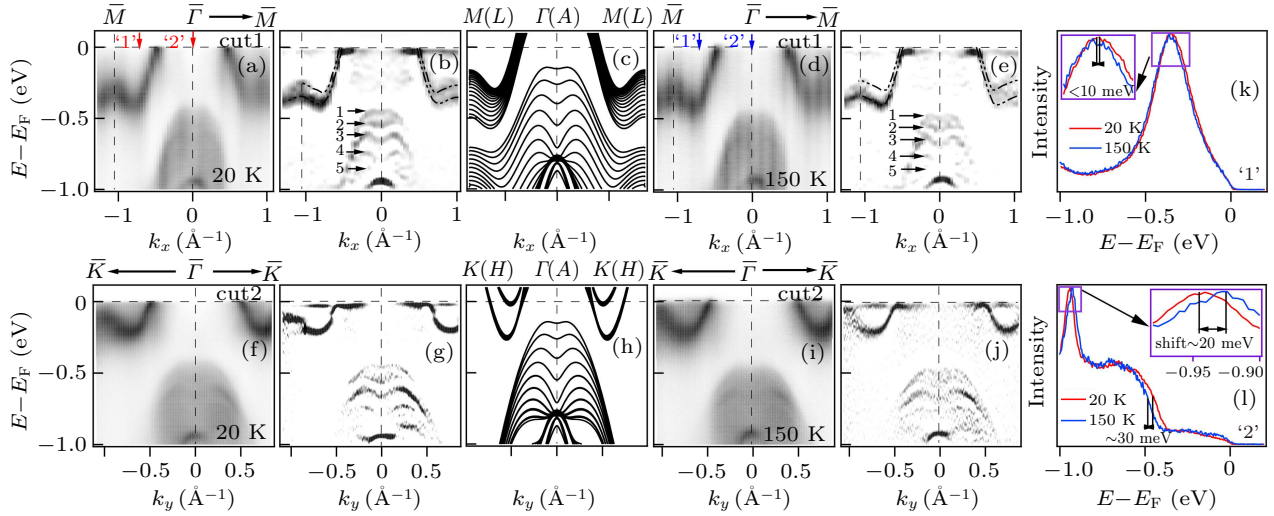


Fig. 3. Electronic structure along high-symmetry cuts. (a), (b) Intensity plot and the corresponding second derivative plot along the $\bar{\Gamma}$–$\bar{M}$ direction (cut #1 in Fig. 1(e)) at $T = 20$ K, the black dotted-lines are guides to the eye. (c) Slab calculation along Γ–M. (d), (e) Same as (a), (b), but recorded along the $\bar{\Gamma}$–$\bar{M}$ direction at $T = 150$ K. (f), (g) Intensity plot and corresponding second derivative plot along $\bar{\Gamma}$–$\bar{K}$ direction (cut #2 in Fig. 1(e)) at $T = 20$ K. (h) Slab calculations along Γ–K. (i), (j) Same as (f), (g) recorded at $T = 150$ K. (k), (l) EDC plots in CDW and normal phase at the momentum marked by '1' and '2' in (a) and (d), corresponding to $\frac{2}{3}\overline{\Gamma M}$ and $\bar{\Gamma}$, respectively.

In order to study the band structure under the influence of surface band bending, we performed the band structure calculations with a 21-layer slab, and plot the results along with high symmetry lines in Figs. 3(c) and 3(h). The slab calculation reproduces the sub-bands qualitatively in agreement with our experimental results. The separations of γ subbands are more pronounced than the other bands, in agreement with the observations. This larger separation is due to the lower ef-

fective mass along the quantization dimension (c-axis), which can be seen from the dispersion along Γ–A in the bulk band calculation.

To quantitatively study the relationship between the band structure close to the Fermi level and the CDW transition, we have traced the three bands, α, β, and γ as noted in bulk band calculation in Fig. (b), to view their changes with temperature. The measured CDW/normal state band dispersions are illustrated in Figs. 3(a)/3(d) and 3(f)/3(i), along $\bar{\Gamma}$–$\bar{M}$ and $\bar{\Gamma}$–$\bar{K}$, respectively. At the low temperature, in spite of the shadow bands caused by the 3×3 reconstruction and the opening of CDW gaps close to E_F, the bands show no noticeable energy shift compared with the normal state. In contrast, the quantized γ sub-bands shift upward while the bulk band of Γ-certer shifts downward with the temperature decrease. The binding energy of the topmost sub-band shifts upward by about 30 meV, from $E_B \sim 485$ meV at $T = 150$ K to $E_B \sim 455$ meV at $T = 20$ K which is beyond the experimental resolution, and so are the following sub-bands. The bulk band of Γ-center shifts downward by about 20 meV, from $E_B \sim 0.92$ eV at $T = 150$ K to $E_B \sim 0.94$ eV at $T = 20$ K. In order to compare the energy shift of the bands, we overlay the EDCs at below and above T_{CDW} at points marked as '1' and '2' in Figs. 3(a) and 3(d), and show them in Figs. 3(k) and 3(l), respectively. From Fig. 3(k), no band shift is observed across the T_{CDW} for α and β bands within the energy resolution, while the quantized sub-bands of γ and bulk band at Γ-center show a clear shift with temperature changes.

We further perform the k_z-dependent measurements in ΓM–AL plane by varying the photon energy, covering more than one BZ along k_z. Figure 4(a) shows the integrated spectra intensity plot around E_F as a function of k_x and k_z, defined as cut #1 in Fig. 1(e). The α, β bands are nearly degenerate and show little dispersion along k_z, confirming the 2D like characters of the bands. We also show the band dispersion along M–L and Γ–A, labeled as cut #3 and cut #4, in Figs. 4(b) and 4(c), respectively. The k_z value is converted with the inner potential $V_0 = 17$ eV empirically to best fit the dispersion. Figure 4(b) shows the ARPES intensity plot along the M–L line, a clear dispersion along k_z at BZ boundary confirms the periodic variation of electronic states. The insets show EDCs at high symmetry points (i.e., M and L), where α and β bands split at M and nearly degenerate at L, in agreement with the bulk band calculation shown in Fig. 1(b).

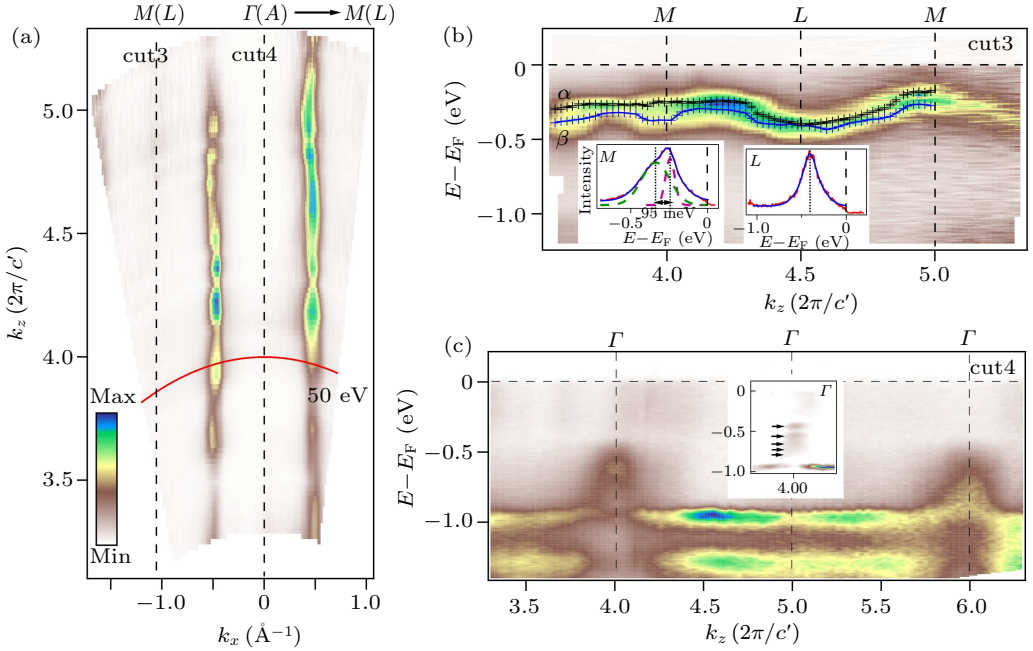


Fig. 4. Photon-energy-dependent band dispersion of 2H-$TaSe_2$. (a) Integrated ARPES intensity map within $E_F \pm 10$ meV in the $h\nu$–$k_\parallel$ plane, where $k_\parallel$ is oriented along the Γ–M (A–L) direction, recorded with various photon energies. (b) ARPES intensity plot along the M–L direction, from cut #3 in Fig. 4(a), the markers are guided to the eyes. Insets show multiple Gaussian peaks fit the EDCs at high symmetry points M and L, respectively. (c) ARPES intensity plot along the Γ–A direction, cut #4, taken with photon energies covering a k_z range over 2 BZs. Inset shows a zoom-in second derivative plot at Γ point.

Figure 4(c) shows the intensity plot along the Γ–A–Γ line over more than two BZs. Besides the flat dispersionless band located at about 1 eV below E_F, the most striking feature is a dispersive band around Γ, with an energy range 0.5–0.9 eV. Closer investigation shows quantized energy levels around Γ, with the band top at about 430–460 meV below E_F, in agreement with the in-plane observations. Due to the existence of quantized states, we can only roughly estimate the band dispersion and extract the band mass along k_z direction $m_z^* \approx 0.06 m_e$, much lighter than those in-plane values. Most of the time, the 2H-$TaSe_2$ was considered as a quasi-2D system, and the CDW was studied in a two-dimensional approach.

Our data suggest that a simple two-dimensional approximation may not be sufficient.

It has been a long-standing puzzle that the γ band is absent and only two hole-like bands in the BZ center are observed. For a band with fast dispersion and light effective mass along the c-axis, the band bending effect, which is caused by the breaking of translation symmetry at the surface, will make the quantization more observable and hinder the observation of the bulk band. From the bulk band calculation (Fig. 1(b)), the γ band disperses rapidly along Γ–A, with relatively flat in-plane dispersion. As aforementioned slab calculation, the quantized states are located at higher binding energies than the bulk band calculation. In contrast, the quantization of α, β bands is not as clear as that of γ band due to slower dispersion and higher effective mass along the c-axis. This can be seen from the less separation of the states in the slab calculations. From the comparison between the bulk band and the slab calculations, in addition to the consistency between ARPES measurement and slab calculation, we safely "recover" a missing bulk band in 2H-$TaSe_2$ in the vicinity of E_F centered at 3D BZ center, with fast dispersion along k_z.

The mechanism of CDW in TMDs remains no consensus due to its complexity. The weak coupling 2D FS-nesting assumption has failed since there is no clear connection of FSs with the CDW vector ($Q_{CDW} = \frac{2}{3}\Gamma M$).[32,45] Strong electron–phonon coupling[30] and scattering between saddle points were proposed to understand the mechanism in 2H-$TaSe_2$.[22–24] However, the pseudogap,[20,21] and temperature dependent dc resistivity[35,44] in TMD are still not fully understood. The preformed excitonic liquid theory was proposed and explained these aforementioned phenomena and suggested an electronically driven CDW in 2H-$TaSe_2$.[49] When the preformed exciton in normal state condenses and becomes coherent, the excitonic interaction causes the shifts of the valence band top position.[49]

Based on the observation of the quantized states, and the DFT and slab calculations, we "recover" the bulk γ band with band top near E_F and a relatively flat in-plane dispersion around the 3D BZ center. Since the quantized states respond with the CDW transition, they could participate in or influence by the formation of CDW. As a surface-sensitive measurement, ARPES observation of the bulk Γ band is hindered by the quantization, and we can only observe the quantized states at the top few layers. In order to confirm if the shift is a CDW related bulk band character or a chemical-shift of the quantized surface state, bulk sensitive measurement such as x-ray ARPES is needed. The band shift of γ band with temperature is inconsistent with the FS nesting, electron–phonon coupling, or preformed exciton liquid scenario.[29,57,59] The understanding of the shift with temperature remains a challenge at the moment, it may cast new perspectives in understanding the CDW mechanism. We expect further bulk sensitive measurement and a better theoretical explanation for this phenomenon in the future.

4. Summary

In conclusion, we measured the band structure of 2H-$TaSe_2$ and measured the temperature and angular dependence of the CDW gap variation. We have observed quantized states in single crystal 2H-$TaSe_2$ for the first time. We studied the in-plane and k_z dependence of the band dispersion and found out the quantization from a previous "missing" band, which is close to Fermi energy in Γ–M–K plane and highly dispersive along k_z. That quantization at the surface results from the band bending due to the surface electron rearrangement and the light carriers' effective mass of the band along Γ–A direction. The band shifts upward with the decrease of temperature into the CCDW state, and the unusual shift is mostly related to the CDW transition. Further bulk sensitive measurement of γ band is needed and it may pave an avenue to understand the CDW in 2H-TMD materials.

Acknowledgements

The authors thank Qiang Han for valuable discussions. Y. H. was supported by the CAS Pioneer Hundred Talents Program (type C). Work at Brookhaven National Laboratory was supported by US DOE, Office of Science, Office of Basic Energy Sciences (DOEBES), under Contract No. DE-SC0012704 (materials synthesis).

References

[1] Santander-Syro A F, Copie O, Kondo T, Fortuna F, Pailhes S, Weht R, Qiu X G, Bertran F, Nicolaou A, Taleb-Ibrahimi A, Le Fevre P, Herranz G, Bibes M, Reyren N, Apertet Y, Lecoeur P, Barthlmy A and Rozenberg M J 2011 *Nature* **469** 189

[2] Meevasana W, King P D C, He R H, Mo S K, Hashimoto M, Tamai A, Songsiriritthigul P, Baumberger F and Shen Z X 2011 *Nat. Mater.* **10** 114

[3] Plumb N C, Salluzzo M, Razzoli E, Mnsson M, Falub M, Krempasky J, Matt C E, Chang J, Schulte M, Braun J, Ebert H, Minr J, Delley B, Zhou K J, Schmitt T, Shi M, Mesot J, Patthey L and Radovi M 2014 *Phys. Rev. Lett.* **113** 086801

[4] Wang Z, McKeownWalker S, Tamai A, Wang Y, Ristic Z, Bruno F Y, de la Torre A, Ricc S, Plumb N C, Shi M, Hlawenka P, Snchez-Barriga J, Varykhalov A, Kim T K, Hoesch M, King P D C, Meevasana W, Diebold U, Mesot J, Moritz B, Devereaux T P, Radovic M and Baumberger F 2016 *Nat. Mater.* **15** 835

[5] Abe S, Inaoka T and Hasegawa M 2002 *Phys. Rev. B* **66** 205309

[6] King P D C, Veal T D and McConville C F 2008 *Phys. Rev. B* **77** 125305

[7] King P D C, Veal T D, McConville CF, Ziga-Prez J, Muoz-Sanjos V, Hopkinson M, Rienks E D L, Fuglsang Jensen M and Hofmann Ph 2010 *Phys. Rev. Lett.* **104** 256803

[8] Hirahara T, Nagao T, Matsuda I, Bihlmayer G, Chulkov E V, Koroteev Y M and Hasegawa S 2007 *Phys. Rev. B* **75** 035422

[9] Matsuda I, Ohta T and Yeom H W 2002 *Phys. Rev. B* **65** 085327

[10] Nagamura N, Matsuda I, Miyata N, Hirahara T, Hasegawa S and Uchihashi T 2006 *Phys. Rev. Lett.* **96** 256801

[11] Ohtomo A and Hwang H Y 2004 *Nature* **427** 423

[12] Thiel S, Hammerl G, Schmehl A, Schneider C W and Mannhart J 2006 *Science* **313** 1942
[13] Klitzing K V, Dorda G and Pepper M 1980 *Phys. Rev. Lett.* **45** 494
[14] Tsui D C, Stormer H L and Gossard A C 1982 *Phys. Rev. Lett.* **48** 1559
[15] Reyren N, Thiel S, Caviglia AD, Kourkoutis LF, Hammerl G, Richter C, Schneider CW, Kopp T, Retschi A S, Jaccard D, Gabay M, Muller D A, Triscone J M and Mannhart J 2007 *Science* **317** 1196
[16] Brinkman A, Huijben M, van Zalk M, Huijben J, Zeitler U, Maan J C, van der Wiel W G, Rijnders G, Blank D H A and Hilgenkamp H 2007 *Nat. Mater* **6** 493
[17] Zhang Z and Yates J T 2012 *Chem. Rev.* **112** 5520
[18] Roch J G, Froehlicher G, Leisgang N, Makk P, Watanabe K, Taniguchi T and Warburton R J 2019 *Nat. Nanotechnol.* **14** 432
[19] Shen D W, Xie B P, Zhao J F, Yang L X, Fang L, Shi J, He R H, Lu D H, Wen H H and Feng D L 2007 *Phys. Rev. Lett.* **99** 216404
[20] Borisenko S V, Kordyuk A A, Yaresko A N, Zabolotnyy V B, Inosov D S, Schuster R, Bchner B, Weber R, Follath R, Patthey L and Berger H 2008 *Phys. Rev. Lett.* **100** 196402
[21] Li Y W, Jiang J, Yang H F, Prabhakaran D, Liu Z K, Yang L X and Chen Y L 2018 *Phys. Rev. B* **97** 115118
[22] Rice T M and Scott G K 1975 *Phys. Rev. Lett.* **35** 120
[23] Liu R, Olson C G, Tonjes W C and Frindt R F 1998 *Phys. Rev. Lett.* **80** 5762
[24] Liu R, Tonjes W C, Greanya V A, Olson C G and Frindt R F 2000 *Phys. Rev. B* **61** 5212
[25] Whangbo M H and Canadell E 1992 *J. Am. Chem. Soc.* **114** 9587
[26] McMillan W L 1977 *Phys. Rev. B* **16** 643
[27] van Wezel J, Nahai-Williamson P and Saxena S S 2010 *Phys. Rev. B* **81** 165109
[28] van Wezel J, Nahai-Williamson P and Saxena S S 2010 *Europhys. Lett.* **89** 47004
[29] Cercellier H, Monney C, Clerc F, Battaglia C, Despont L, Garnier M G, Beck H, Aebi P, Patthey L, Berger H and Forr L 2007 *Phys. Rev. Lett.* **99** 146403
[30] Gorkov L P 2012 *Phys. Rev. B* **85** 165142
[31] Dai J X, Calleja E, Alldredge J, Zhu X D, Li L J, Lu W J, Sun Y P, Wolf T, Berger H and McElroy K 2014 *Phys. Rev. B* **89** 165140
[32] Johannes M D and Mazin I I 2008 *Phys. Rev. B* **77** 165135
[33] Li L J, Deng X, Wang Z, Liu Y, Abeykoon M, Dooryhee E, Tomic A, Huang Y N, Warren J B, Bozin E S, Billinge S J L, Sun Y P, Zhu Y M, Kotliar G and Petrovic C 2017 *npj Quantum Materials* **2** 11
[34] Qiao S, Li X, Wang N, Ruan W, Ye C, Cai P, Hao Z Q, Yao H, Chen X H, Wu J, Wang Y Y and Liu Z 2017 *Phys. Rev. X* **7** 041054
[35] Vescoli V, Degiorgi L, Berger H and Forr L 1998 *Phys. Rev. Lett.* **81** 453
[36] Rossnagel K, Rotenberg E, Koh H, Smith N V and Kipp L 2005 *Phys. Rev. B* **72** 121103
[37] Valla T, Fedorov A V, Johnson P D, Xue J, Smith K E and DiSalvo F J 2000 *Phys. Rev. Lett.* **85** 4759
[38] Moncton D E, Axe J D and DiSalvo F J 1977 *Phys. Rev. B* **16** 801
[39] Withers R L and Bursill L A 1982 *Phys. Rev. B* **26** 1469
[40] Wang C, Giambattista B, Slough C G, Coleman R V and Subramanian M A 1990 *Phys. Rev. B* **42** 8890
[41] Galvis J A, Rodire P, Guillamon I, Osorio M R, Rodrigo J G, Cario L, Navarro-Moratalla E, Coronado E, Vieira S and Suderow H 2013 *Phys. Rev. B* **87** 094502
[42] Demsar J, Forr L, Berger H and Mihailovic D 2002 *Phys. Rev. B* **66** 041101
[43] Evtushinsky D V, Kordyuk A A, Zabolotnyy V B, Inosov D S, Bchner B, Berger H, Patthey L, Follath R and Borisenko S V 2008 *Phys. Rev. Lett.* **100** 236402
[44] Ruzicka B, Degiorgi L, Berger H, Gal R and Forr L 2001 *Phys. Rev. Lett.* **86** 4136
[45] Laverock J, Newby D Jr, Abreu E, Averitt R, Smith K E, Singh R P, Balakrishnan G, Adell J and Balasubramanian T 2013 *Phys. Rev. B* **88** 035108
[46] Barnett R L, Polkovnikov A, Demler E, Yin W G and Ku W 2006 *Phys. Rev. Lett.* **96** 026406
[47] Ge Y and Liu A Y 2012 *Phys. Rev. B* **86** 104101
[48] Inosov D S, Zabolotnyy V B, Evtushinsky D V, Kordyuk A A, Bchner B, Follath R, Berger H and Borisenko S V 2008 *New J. Phys.* **10** 125027
[49] Taraphder A, Koley S, Vidhyadhiraja N S and Laad M S 2011 *Phys. Rev. Lett.* **106** 236405
[50] Kresse G and Joubert D 1999 *Phys. Rev. B* **59** 1758
[51] Blchl P E 1994 *Phys. Rev. B* **50** 17953
[52] Kresse G and Furthmller J 1996 *Comput. Mater. Sci.* **6** 15
[53] Kresse G and Hafner J 1993 *Phys. Rev. B* **47** 558
[54] Kresse G and Furthmller J 1996 *Phys. Rev. B* **54** 11169
[55] Perdew J P, Burke K and Ernzerhof M 1996 *Phys. Rev. Lett.* **77** 3865
[56] Klime J, Bowler D R and Michaelides A 2009 *J. Phys.: Condens. Matter* **22** 022201
[57] Rossnagel K 2011 *J. Phys.: Condens. Matter* **23** 213001
[58] Clark OJ, Mazzola F, Feng J, Sunko V, Markovi I, Bawden L, Kim T K, King P D C and Bahramy M S 2019 *Phys. Rev. B* **99** 045438
[59] Kohn W 1967 *Phys. Rev. Lett.* **19** 439